

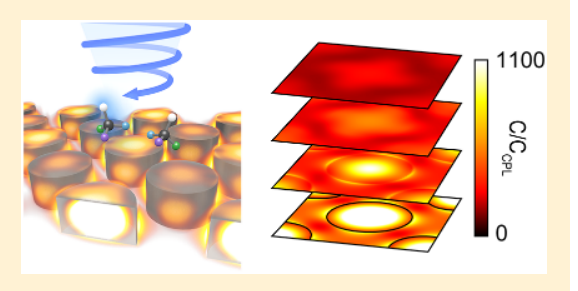
High Quality Factor Dielectric Metasurfaces for Ultraviolet Circular Dichroism Spectroscopy

Jack Hu,* [®] Mark Lawrence,® and Jennifer A. Dionne*

Department of Materials Science and Engineering, Stanford University, Stanford, California 94305, United States

Supporting Information

ABSTRACT: Chiral-optical spectroscopies, such as circular dichroism, are critical in the biomedical, pharmaceutical, and agrochemical industries for revealing structural information about molecules and determining the purity of chemical samples. Emerging nanophotonic platforms have been shown to increase the intrinsically weak interaction between circularly polarized light and chiral molecules through the concentration of the local density of optical chirality, C. However, enhancements in C have been limited to infrared and visible frequencies, while the chiral absorption features of most small molecules are in the ultraviolet. Furthermore, achievable C enhancements in nanophotonic



systems remain relatively low, especially when averaged across the sample volume. Here, we use full-field simulations to design a high quality factor (high Q) diamond metasurface that enhances C by over 3 orders of magnitude in the ultraviolet regime. The diamond nanostructures enable ultraviolet Mie resonances while a biperiodic disk lattice activates high Q resonances that significantly increase the electromagnetic field intensities. When a high Q electric dipole and magnetic dipole mode are spatially and spectrally overlapped, a Kerker-like condition emerges that enables uniform sign C enhancements that are locally as high as 1130-fold. Even when averaged across the unit cell and 40 nm away from the surface, enhancements in C exceed 100-fold. We show how the quality factor and C can be further tuned by adjusting the structural asymmetry via the diameter of set in the biperiodic lattice. Our results pave the way for ultrasensitive chiral spectroscopy and efficient light-mediated enantiomer separation.

KEYWORDS: optical chirality, circular dichroism, dielectric metasurfaces, high quality factor, ultraviolet

hirality is a physical descriptor for a pair of objects that are mirror images of each other, but not superimposable. In living matter, molecular chirality significantly dictates the function of many biomolecules, including proteins, amino acids, enzymes, and hormones.1 For example, physiologically active amino acids appear as L-enantiomers while trace amounts of D-amino acids can mark the onset of organ failure or neurodegenerative diseases.^{2,3} Synthetic chemicals such as pharmaceuticals and agrochemicals can also exhibit chirality, with opposite enantiomers having distinct interactions with biological life.4,5

The enantiospecific interactions between chiral molecules and chiral light offers a versatile method to detect and distinguish enantiomers. This phenomena is utilized in circular dichroism (CD) spectroscopy, where the differential absorption of an enantiomer illuminated with right- and left-circularly polarized (RCP/LCP) light is measured. 6 CD spectroscopy can both determine the secondary structure of chiral molecules and the purity of a chiral solution. However, the chiroptical response of most small molecules is intrinsically weak; the differential RCP/LCP absorption is generally 10^{-3} to 10^{-6} times smaller than the absolute absorption, necessitating high analyte concentrations and long integration times.^{7,8}

Recent developments in novel nanophotonic materials have produced platforms with favorable properties for highly sensitive chiral molecule detection. These metamaterials are generally designed to provide large local concentrations of optical chirality, C, defined as^{9,10}

$$C = -\frac{\omega}{2c^2} Im(E^* \cdot H) = -\frac{\omega}{2c^2} |E||H| cos(\phi_{iE,H})$$
 (1)

where E and H represent the complex electric and magnetic fields, and ω , ϵ_0 , and μ_0 are the angular frequency of light, permittivity of free space, and permeability of free space, respectively. The ellipticity of the electromagnetic fields is captured by ϕ_{iEH} , which describes the phase angle between iE and H. For circularly polarized light (CPL) in vacuum, $\cos(\phi_{iE,H}) = \pm 1$ and $C_{CPL} = \pm \frac{\epsilon_0 \omega}{2c} E_0^2$, where E_0 is the incident electric field amplitude. The differential absorption of RCP and LCP by an enantiomer, $\Delta \varepsilon$, is proportional to the local C.^{11,12} Thus, designing platforms that concentrate electromagnetic fields while creating or maintaining circular polarized states provides a means to increase the chiroptical response of molecules.

In the past, both plasmonic resonances in metallic structures and Mie resonances in high-refractive-index dielectric materials have been engineered for this purpose. Calculated enhance-

Received: September 19, 2019 Published: November 13, 2019

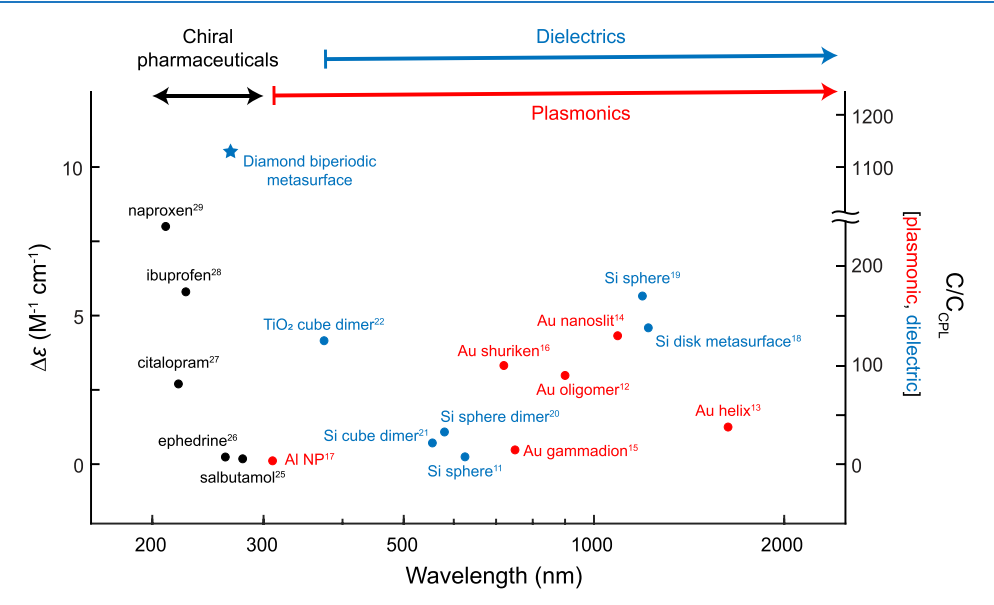


Figure 1. Calculated optical chirality enhancements in plasmonic and dielectric nanophotonic platforms compared with differential RCP/LCP absorption, $\Delta \varepsilon$, of small molecule pharmaceuticals. The contribution of this work is marked with a star. Note: C enhancements for these nanostructures were calculated for specific design parameters and wavelengths, but many designs feature enhancements that can be tuned via geometrical parameters across the visible and IR spectrum.

ments in C upward of 150-fold greater than that of CPL have been demonstrated for metallic helices, gammadions, shurikens, and twisted nanoparticle assemblies, as well as dielectric spheres, cubes, and disks. 11-22 Using these systems, augmented chiral detection has been experimentally achieved on large molecules with chiroptical bands at visible and infrared (IR) frequencies. 15,23,24 However, the chiral response of most industrially relevant small molecules are in the ultraviolet (UV) regime as illustrated in Figure 1. 25-29 While certain plasmonic and quantum dot systems can enhance nonresonant tails or induce CD signals at visible frequencies, molecular information is convoluted in the overall system response. 17,24,30,31

To improve the performance of chiral sensing platforms, novel metamaterials must be developed with resonances overlapping the chiral molecular absorption features in the UV regime. Enhancing C in the UV requires materials with low losses, as absorption by the nanostructures dampens resonant enhancements and induces a background signal in CD measurements.³² Although UV transparent dielectrics could be utilized with previous nanophotonic designs, these systems are inherently limited by low quality factor (Q) resonances (Q ~ 10) that only weakly concentrate electromagnetic fields.^{18,21,33} This challenge is further exacerbated by the lower refractive indices of UV materials. Furthermore, many chiral sensors produce nonuniform chiral fields or rely on field confinement in tight gaps, where the chiroptical response of molecules is only enhanced in certain locations on the nanostructures.

In this work, we introduce the design of high quality factor (high Q) diamond metasurfaces for enhanced CD in midultraviolet frequencies. The use of diamond enables UV Mie resonances while our high Q design increases the electromagnetic field intensities and optical chirality densities by orders of magnitude. We consider a metasurface consisting of a biperiodic disk lattice where the asymmetry in adjacent disks allows for free-space coupling into high Q resonances. The tuning of asymmetric electric and magnetic dipole modes

enhances the optical chirality density over 3 orders of magnitude locally. Importantly, optical chirality enhancements are of a single handedness and still exceed 2 orders of magnitude averaged across a plane 40 nm away from the metasurface. This global enhancement of C is a desired property for CD spectroscopy measurements where small molecules will be randomly distributed around the nanostructures. Furthermore, we show that altering the degree of asymmetry in the disk lattice controls the resonant Q factors and allows for C enhancements spanning multiple orders of magnitude.

To enhance the electromagnetic density of chirality, C, we first consider a diamond disk metasurface. Diamond was chosen as the studied material system due to its relatively high refractive index (n ~ 2.6) and negligible losses down to $\lambda \sim 240$ nm. Furthermore, advances in fabrication techniques have produced high-quality nanoscale diamond structures. 34,35 However, other UV transparent materials with relatively high refractive indices such as aluminum nitride or hafnium oxide could also be considered. We base our nanophotonic platform on a dielectric disk metasurface where the nanoantennas support both electric and magnetic Mie resonances that can be independently tuned in relation to each other via the disk aspect ratio. 36,37

Using full-field finite difference time domain simulations, we first calculate the total fields from a square array of disks illuminated with CPL at normal incidence. The dielectric structures are calculated with the optical properties of diamond including loss, 38 and are embedded in a background refractive index of n=1 (see Supporting Information and ref 18 for substrate and superstrate effects). The metasurfaces have dimensions of height h=60 nm, lattice parameter a=200 nm, and diameters ranging from d=132 nm to d=156 nm (Figure 2a). The incident light is an LCP plane wave propagating in the -z direction.

In Figure 2b for the curve corresponding to diameter d = 156 nm, we see two resonance dips at $\lambda = 286$ and 270 nm. These two modes are an electric dipole p and magnetic dipole

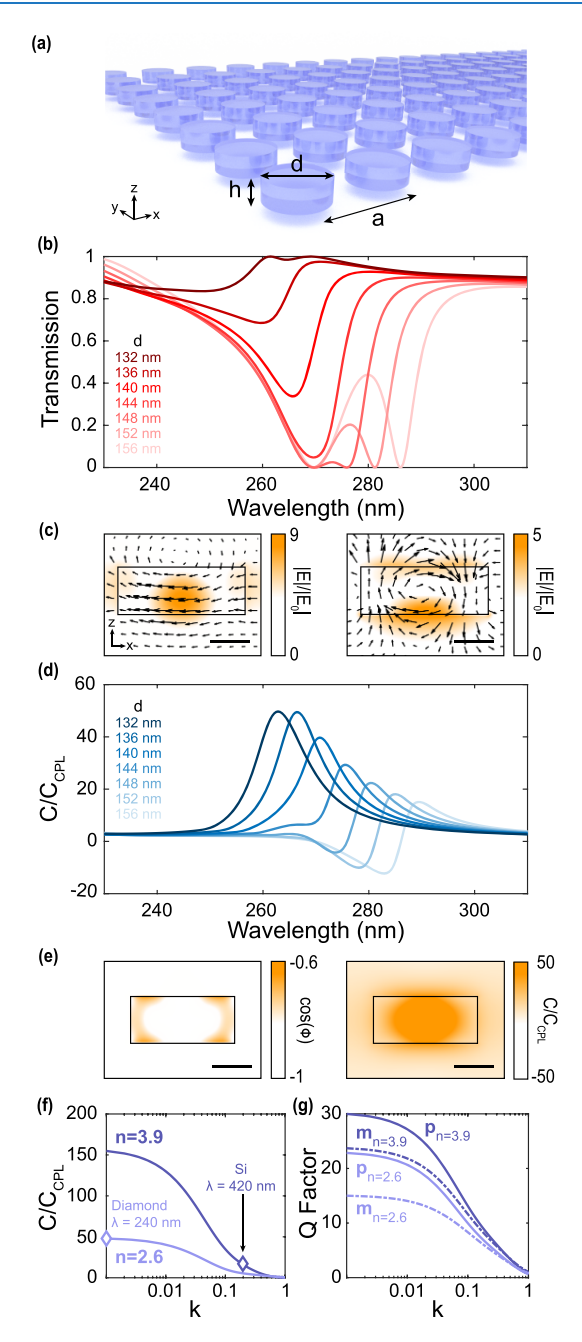


Figure 2. (a) Schematic of dielectric disk metasurface. (b) Transmission spectra of a diamond metasurface with h = 60 nm, a = 200 nm, and d = 132–156 nm. (c) Electric field distributions for the electric and magnetic dipolar modes. Scale bars are 50 nm. (d) Spectra of C/ C_{CPL} for varying disk diameters. (e) Spatial distributions of $\cos(\phi_{iE,H})$ and C enhancements, for a metasurface with d/h = 2.2 (d = 132 nm) at λ = 263 nm. (f) Maximum local C enhancements as a function of the imaginary part of the refractive index, k, for silicon (n = 3.9) and diamond (n = 2.6) metasurfaces. (g) Q factors of the electric and magnetic dipole resonances in silicon and diamond.

m, as seen from the field distributions in Figure 2c. When the disk aspect ratio (d/h) is tuned by altering the diameter, p and m shift frequencies in relation to each other. At an aspect ratio of d/h = 2.2 (d = 132 nm) the dipolar modes are spectrally overlapped and exhibit a Kerker condition where the transmission approaches unity.³⁹ When the metasurface is operating at the Kerker condition, the scattered fields from the

structure preserve the helicity of the incident CPL, a property that is ideally suited for enhancing optical chirality.⁴⁰ Our group has previously shown this effect for the IR regime in silicon disk metasurfaces to obtain maximum local C enhancements of 150-fold compared to freely propagating CPL. 18 We now utilize this condition in the ultraviolet. Figure 2d shows the maximum local enhancement of C external to the diamond structures as the disk aspect ratio is tuned to d/h = 2.2 (d = 132 nm). At this aspect ratio, the maximum local optical chirality enhancement outside of the disks is 49-fold greater than that of CPL. In Figure 2e, the spatial distribution of $\cos(\phi)$ indicates that the E and H scattered fields have a $\pi/2$ phase shift and maintain the incident circular polarization. The circularly polarized near fields in combination with the resonant E and H concentrations produce strong C enhancements in the disk that extend into the surrounding medium. The C enhancements around the metasurface are of the same handedness, which is beneficial for experimental CD measurements, where it is difficult to localize molecules at specific locations around the nanostructures.

While spectral overlap of p and m modes is an effective strategy for increasing C, these enhancements can be limited by the optical properties of the dielectric material. For comparison, we optimize two sets of disk metasurfaces with fixed refractive indices of n = 3.9 (representative of silicon in the visible) and n = 2.6 (representative of diamond in the UV). The disk aspect ratios for these two sets are d/h = 2.35 for silicon and d/h = 2.2 for diamond. The maximum local optical chirality is then calculated as the imaginary component of the refractive index, k, is increased (Figure 2f). Additionally, Figure 2g shows the quality factor of both p and m, as calculated from the line widths of the electric field intensity $|E|^2$ and magnetic field intensity $|H|^2$ at the center of the disks, respectively. The Q factor of the resonances correlates with the field intensities produced around the nanostructures and consequently the highest attainable C enhancements. Figure 2f,g indicates that higher refractive index materials can produce a significantly larger enhancement in C, but that material absorption quickly dampens the resonances and diminishes the chiral fields. At wavelengths longer than $\lambda = 1100$ nm, silicon is lossless and exhibits a maximum C enhancement of 150-fold. However, as the imaginary part of the silicon refractive index increases, C rapidly decreases until there is no significant enhancement below ~400 nm. Diamond metasurfaces can only achieve a maximum C increase of 49-fold, but are lossless until ~240 nm. These insights suggest that designing a metasurface with higher Q modes in a lossless material would allow for even greater optical chirality increases in the UV.

In order to increase the quality factors of our resonant modes and, consequently, the local field concentrations, we utilize dark modes, coupling into them from the far field via asymmetries in the disk array. We now consider a biperiodic metasurface where a unit cell consists of two disks with diameters $d + \frac{\Delta}{2}$ and $d - \frac{\Delta}{2}$ arranged in a square checkerboard lattice (Figure 3a). We describe the geometric difference between adjacent disks through the asymmetry parameter, α :

$$\alpha = \frac{\Delta}{d} \tag{2}$$

In Figure 3b, we consider a symmetric ($\alpha = 0$) and asymmetric ($\alpha = 0.1$) diamond metasurface with dimensions h = 60 nm, a = 200 nm, and d = 92 nm. The two broad dips

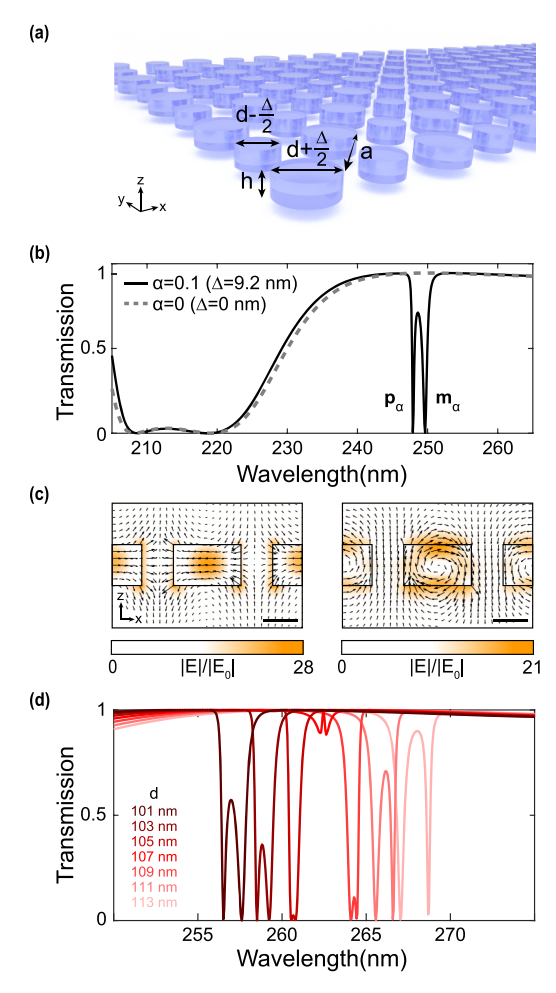


Figure 3. (a) Schematic of biperiodic dielectric disk metasurface. (b) Transmission spectra of symmetric ($\alpha=0$) and asymmetric ($\alpha=0.1$) diamond disk metasurfaces. The metasurfaces have dimensions a = 200 nm, h = 60 nm, and d = 92 nm. (c) Electric field distributions for the asymmetric electric and magnetic dipolar modes. Scale bars are 50 nm. (d) Transmission spectra of asymmetric disk metasurfaces ($\alpha=0.1$) with h = 60 nm and diameters d = 101 to 113 nm.

around 210 and 220 nm correspond to the normal p and m modes seen previously in metasurfaces where the disk diameters are all equal. When we introduce a disk asymmetry to form a biperiodic lattice, two sharp resonance features appear in the transmission spectra. These high Q resonances are also dipole-like as seen in the electric field distributions in Figure 3c. One of these modes has an electric character (p_{α}) , while the other is magnetic (m_{α}) . However, dipoles in neighboring disks are oscillating out of phase. The asymmetry suppresses the interaction of the resonances with free space, leading to longer resonance lifetimes and higher quality factors. When the diameters of the disk are offset by 10% ($\alpha = 0.1$), the Q factors of p_{α} and m_{α} are ~1000 and ~500, respectively. The extended resonant lifetimes produce large field enhancements within the disks, $|E|/|E_0| \sim 30$ and $|H|/|H_0| \sim 65$. We chose $\alpha =$ 0.1, where $\Delta \sim 10$ nm, as these dimensions are on the order of achievable features with state of the art diamond fabrication techniques. 42 However, the geometric asymmetry between neighboring disks can be tuned to further increase the Q factor of these resonances (vide infra).

Similar to symmetric disk metasurfaces, changing the disk aspect ratios shifts the resonant frequencies of the asymmetric dipole modes. Increasing the aspect ratio of both disks in a biperiodic lattice while maintaining a constant α causes the high Q electric and magnetic dipoles to shift in relation to each other. Figure 3d shows the transmission spectra of biperiodic diamond metasurfaces with lattice parameter $\alpha = 200$ nm, height $\alpha = 60$ nm, asymmetry parameter $\alpha = 0.1$, and center diameter varying from $\alpha = 101$ to 113 nm (a finer parameter sweep is included in the Supporting Information). Increasing the disk diameter creates a larger frequency shift in $\alpha = 100$ nm. At this condition, we see unity transmission as backscattering is suppressed in a Kerker-like condition involving high Q dipolar resonances.

Tailoring C with the asymmetric dipolar modes p_{α} and m_{α} is analogous to the results shown in Figure 2 utilizing symmetric dipolar modes p and m. The local maximum C enhancements external to the disks are calculated for the biperiodic metasurfaces as the diameter is varied (Figure 4a). The optical chirality density is most strongly enhanced when the modes are spectrally overlapped for a metasurface with d = 107 nm and reach a peak value enhancement of >1100-fold. Furthermore, the spatial distribution of the phase difference between the electric and magnetic fields when the modes are overlapped shows that the incident polarization of the LCP wave is largely preserved in the scattered field and $\cos(\phi)$ is negative in sign for all space (Figure 4b).

Since the circular polarization state of the incident wave is largely maintained, C is increased for a single handedness and enhancements persist throughout the near field of the metasurface. The spatial distribution of C in Figure 4c shows that C is most highly concentrated inside the diamond nanodisks where the electromagnetic field intensities of the dipolar modes are strongest and decay away from the surface of the disks. In Figure 4d, we show a three-dimensional visualization of the optical chirality enhancement surrounding the metasurface along with cut planes at different z heights (z = 0 describes the plane that intersects the center of the disks). In all planes, C enhancements are of a single handedness. The largest values of C are located at hotspots on the top surface of the disks (z = 30 nm) and along four lobes around the radial face of the disks (z = 0 nm) where enhancements of ≥ 1000 fold are observed. Additionally, large values of C/C_{CPL} persist in the space between nanostructures with a minimum of ~230.

To quantify the large enantiospecific enhancements seen in the volume surrounding the metasurface, we consider local and averaged optical chirality across various z slices. In Figure 4e, C_{local} plots the maximum value of the local optical chirality enhancement along a particular z height. We see at z = 0 nm, the plane that cuts through the center of the disk array, the maximum value of C/C_{CPL} external to the disks is 1000 and enhancements decline until z = 30 nm at the top surface of the disks where $C/C_{CPL} = 1130$. From z = 30 nm, enhancements decay exponentially away from the surface of the disk array. This trend is identical in both the +z and -z direction as the C enhancements are mirror symmetric about the z = 0 nm plane (Supporting Information). The optical chirality enhancement external to the disks averaged across a plane is considered in the C_{ave} curve. We see that, when C enhancements are considered in all the space between disks (z = 0 to 30 nm), the average optical chirality density exceeds 400-fold. Even above the metasurface, the average C increase across a plane is greater

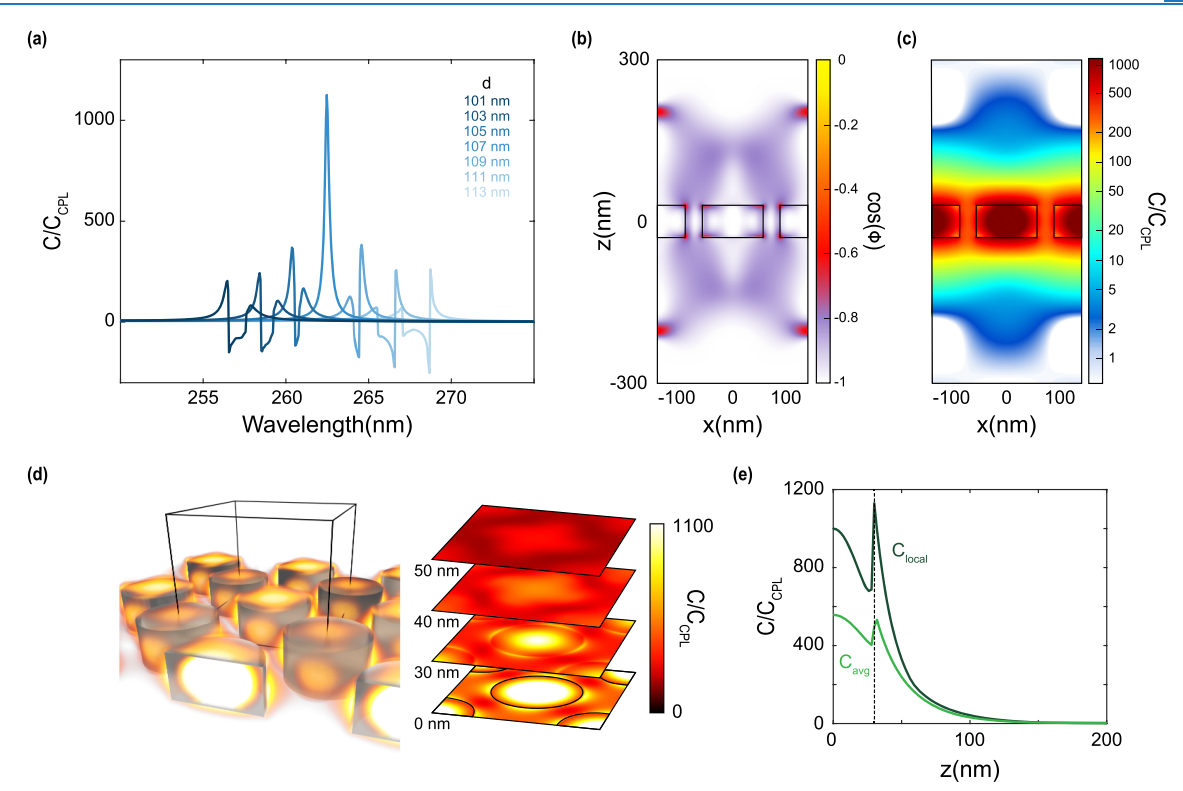


Figure 4. (a) Maximum local optical chirality for high Q disk metasurfaces (α = 0.1) with h = 60 nm and diameters d = 101 to 113 nm. (b) Spatial distribution of the phase between E and H, $\cos(\phi)$, for a metasurface with d = 107 nm. (c) Logarithmic scaled distribution of C for a metasurface with d = 107 nm. (d) Three-dimensional rendering of the near field optical chirality enhancements in an asymmetric disk metasurface (α = 0.1, d = 107 nm) and x-y cut planes at various z heights in a single unit cell. (e) z height dependence of local (C_{local}) and plane averaged (C_{avg}) optical chirality enhancements. The dashed line marks the top surface of the disks at z = 30 nm.

than 100-fold until z = 70 nm. This result illustrates the advantage of utilizing spectrally and spatially aligned electric and magnetic dipole resonances to concentrate the electromagnetic fields while maintaining a single handedness of polarization in the scattered fields. When p_α and m_α are detuned, the individual resonances still produce large local concentrations of C, but of opposite signs, leading to minimal averaged enhancements (Supporting Information). In the Supporting Information, we also show that even when the background refractive index is increased to n = 1.5 in order to represent a substrate and superstrate, the high Q modes p_α and m_α are still present and $C/C_{CPL} \geq 1000$ can be achieved.

Finally, we note that our biperiodic diamond lattice can be tailored to increase Kuhn's dissymmetry factor, g, for enantiospecific photolysis or photosynthesis of chiral molecules. This factor describes the efficiency with which a chiral molecule absorbs RCP versus LCP. Our diamond metasurfaces can enhance glocally by 35-fold compared to CPL (Supporting Information). Assuming first order kinetics, this enhancement can impact the asymmetric photodecomposition of an azidoamide molecule (g = 0.024), 43,44 producing a solution with a 10% enantiomeric excess at a product yield of 79% compared to 0.02% with no metasurface.

While we have shown that large C enhancements can be achieved in metasurfaces with a fixed $\alpha=0.1$, the structural asymmetry can be used as an additional tuning parameter to control the resonant lifetimes of the asymmetric electric and magnetic dipole resonances. As seen in Figure 5a, the Q factor of p_{α} and m_{α} increase as the diameter offset between neighboring disks is decreased. The dependence of the Q

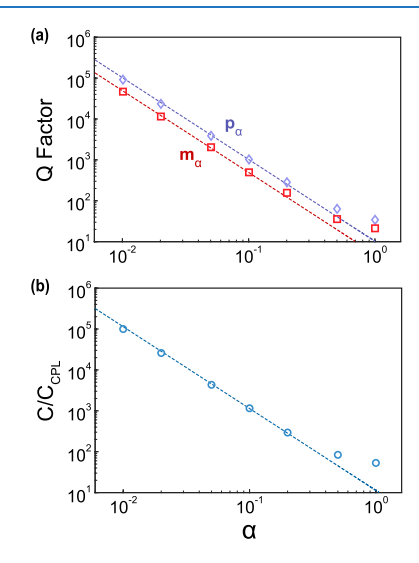


Figure 5. (a) Quality factors of the asymmetric electric p_{α} and magnetic m_{α} dipole resonances with varying asymmetry parameter. (b) Maximum local optical chirality enhancements in diamond biperiodic metasurfaces with varying asymmetry parameters. The dashed lines represent functions of the form B/α^2 , where B is a constant.

factor on small structural deviations, such as α , has been previously described in metasurfaces through temporal coupled-mode theory and perturbation theory:

$$Q = \frac{B}{\alpha^2}$$
 (3)

where B is a constant that depends on the metasurface design. This relationship is only valid for small structural perturbations and we see the trend for the Q factor deviating when α is greater than 0.1 (Figure 5a). If we vary a and spectrally align the p_{α} and m_{α} modes, we also see a similar trend in the maximum local C enhancements (Figure 5b). Tuning the quality factor of the resonant modes in our metasurface allows us to achieve optical chirality enhancements multiple orders of magnitude larger than previously reported nanophotonic sensors, as discussed in Figure 1. Furthermore, the Q factors can be theoretically increased indefinitely as the structural perturbation α is made infinitely small. Therefore, resonant enhancement of the electromagnetic fields and C are mainly limited by the achievable fabrication tolerances and intrinsic absorption. In practical applications, spectral alignment of high Q resonant modes through geometric tuning will also be challenging due to fabrication imperfections. However, resonance frequencies could be further adjusted with gas condensation, temperature control, or electrical tuning methods.48,49

In conclusion, we have introduced metasurfaces that strongly enhance the optical chirality, C, in the midultraviolet wavelength regime. Our platform utilizes dielectric disks, where electric and magnetic dipole resonances can be tuned in relation to each other through the disk aspect ratio. Since conventional high refractive index dielectrics such as silicon are susceptible to losses in the UV, we perform calculations based on diamond resonators. While our study focuses on diamond, these metasurfaces could also be engineered in other UV transparent materials such as aluminum nitride. To increase electromagnetic field intensities, we exploit resonances with higher quality factors. We design a biperiodic disk metasurface, where a geometric asymmetry is introduced in the form of a diameter offset in adjacent nanoantennas. This structural perturbation allows for coupling to high Q asymmetric electric and magnetic dipole resonances. We find that the spectral overlap of these modes produces a Kerker effect that resonantly enhances the near fields while maintaining the polarization of the incident CPL, a condition ideally suited for maximizing C/C_{CPI} . When the difference in diameters of the adjacent disks in our biperiodic lattice is 10%, the local C enhancement exceeds 1000-fold and plane averaged C enhancements 40 nm away from the metasurface exceed 100-fold. We also show that tuning the degree of asymmetry in a biperiodic lattice can produce resonant Q factors and C enhancements spanning multiple orders of magnitude. These enhancements occur for wavelengths between 200 and 300 nm where most chiral small molecules exhibit CD peaks. However, this high Q platform can also be scaled to operate at longer wavelengths for other spectroscopies such as vibrational circular dichroism. Additionally, this design features highly spectrally selective C enhancements that could be utilized in a pixelated metasurface for molecular chirality barcoding.⁵⁰ The ability to control the resonant quality factors and increase optical chirality densities in metasurfaces has the potential for highly sensitive chiroptical spectroscopy as well as efficient enantiomer separation.

ASSOCIATED CONTENT

Supporting Information

The Supporting Information is available free of charge on the ACS Publications website at DOI: 10.1021/acsphotonics.9b01352.

Simulation details, a finer parameter sweep for the biperiodic lattice, discussion of singled handedness vs mixed handedness C enhancements, calculations of a metasurface embedded in a background index of n=1.5, and discussion of Kuhn \$ dissymmetry factor enhancements for asymmetric photolysis (PDF)

AUTHOR INFORMATION

Corresponding Authors

*E-mail: hujack@stanford.edu. *E-mail: jdionne@stanford.edu.

ORCID ®

Jack Hu: 0000-0001-7515-0386

Mark Lawrence: 0000-0002-0822-5453

Notes

The authors declare no competing financial interest.

ACKNOWLEDGMENTS

The authors thank Michelle Solomon, John Abendroth, and Lisa Poulikakos for insightful discussions. The authors gratefully acknowledge the Gordon and Betty Moore Foundation for funding through a Moore Inventors Fellowship. M.L. and J.D. also acknowledge additional funding from an AFOSR PECASE (Grant # FA9550-15-1-0006) and the National Science Foundation (Grant # DMR-1905209).

REFERENCES

- (1) Dobson, C. M. Protein folding and misfolding. Nature 2003, 426, 884–890.
- (2) Kimura, T.; Hamase, K.; Miyoshi, Y.; Yamamoto, R.; Yasuda, K.; Mita, M.; Rakugi, H.; Hayashi, T.; Isaka, Y. Chiral amino acid metabolomics for novel biomarker screening in the prognosis of chronic kidney disease. Sci. Rep. 2016, 6, 26137.
- (3) Lin, C.-H.; Yang, H.-T.; Chiu, C.-C.; Lane, H.-Y. Blood levels of D-amino acid oxidase vs D-amino acids in reflecting cognitive aging. Sci. Rep. 2017, 7, 14849.
- (4) Nguyen, L. A.; He, H.; Pham-Huy, C. Chiral Drugs: An Overview. International Journal of Biomedical Science 2006, 2, 85–100.
- (5) Smith, S. W. Chiral toxicology: It the same thing...Only Different. Toxicol. Sci. 2009, 110, 4-30.
- (6) Barron, L. D. Molecular Light Scattering and Optical Activity; Cambridge University Press, 2009.
- (7) Fasman, G. D. Circular Dichroism and the Conformational Analysis of Biomolecules; Springer, 1996.
- (8) Kelly, S. M.; Jess, T. J.; Price, N. C. How to study proteins by circular dichroism. Biochim. Biophys. Acta, Proteins Proteomics 2005, 1751, 119–139.
- (9) Lipkin, D. M. Existence of a new conservation law in electromagnetic theory. J. Math. Phys. 1964, 5, 696–700.
- (10) Tang, Y.; Cohen, A. E. Optical chirality and its interaction with matter. Phys. Rev. Lett. 2010, 104, 163901.
- (11) García-Etxarri, A.; Dionne, J. A. Surface-enhanced circular dichroism spectroscopy mediated by nonchiral nanoantennas. Phys. Rev. B: Condens. Matter Mater. Phys. 2013, 87, 235409.
- (12) Schäferling, M.; Dregely, D.; Hentschel, M.; Giessen, H. Tailoring Enhanced Optical Chirality: Design Principles for Chiral Plasmonic Nanostructures. Phys. Rev. X 2012, 2, 031010.

(13) Schäferling, M.; Yin, X.; Engheta, N.; Giessen, H. Helical Plasmonic Nanostructures as Prototypical Chiral Near-Field Sources. ACS Photonics 2014, 1, 530–537.

- (14) Hendry, E.; Mikhaylovskiy, R. V.; Barron, L. D.; Kadodwala, M.; Davis, T. J. Chiral Electromagnetic Fields Generated by Array of Nanoslits. Nano Lett. 2012, 12, 3640–3644.
- (15) Hendry, E.; Carpy, T.; Johnston, J.; Popland, M.; Mikhaylovskiy, R. V.; Lapthorn, A. J.; Kelly, S. M.; Barron, L. D.; Gadegaard, N.; Kadodwala, M. Ultrasensitive detection and characterization of biomolecules using superchiral fields. Nat. Nanotechnol. 2010, 5, 783–787.
- (16) Kelly, C.; Khorashad, L. K.; Gadegaard, N.; Barron, L. D.; Govorov, A. O.; Karimullah, A. S.; Kadodwala, M. Controlling Metamaterial Transparency with Superchiral Fields. ACS Photonics 2018, 5, 535–543.
- (17) McPeak, K. M.; van Engers, C. D.; Bianchi, S.; Rossinelli, A.; Poulikakos, L. V.; Bernard, L.; Herrmann, S.; Kim, D. K.; Burger, S.; Blome, M.; Jayanti, S. V.; Norris, D. J. Ultraviolet Plasmonic Chirality from Colloidal Aluminum Nanoparticles Exhibiting Charge-Selective Protein Detection. Adv. Mater. 2015, 27, 6244–6250.
- (18) Solomon, M. L.; Hu, J.; Lawrence, M.; García-Etxarri, A.; Dionne, J. A. Enantiospecific Optical Enhancement of Chiral Sensing and Separation with Dielectric Metasurfaces. ACS Photonics 2019, 6, 43–49.
- (19) Ho, C.-S.; García-Etxarri, A.; Zhao, Y.; Dionne, J. A. Enhancing Enantioselective Absorption Using Dielectric Nanospheres. ACS Photonics 2017, 4, 197–203.
- (20) Zhang, W.; Wu, T.; Wang, R.; Zhang, X. Amplification of the molecular chiroptical effect by low-loss dielectric nanoantennas. Nanoscale 2017, 9, 5701–5707.
- (21) Yao, K.; Liu, Y. Enhancing circular dichroism by chiral hotspots in silicon nanocube dimers. Nanoscale 2018, 10, 8779–8786.
- (22) Yao, K.; Zheng, Y. Near-Ultraviolet Dielectric Metasurfaces: from Surface-Enhanced Circular Dichroism Spectroscopy to Polarization-Preserving Mirros. J. Phys. Chem. C 2019, 123, 11814–11822.
- (23) Vestler, D.; Ben-Moshe, A.; Markovich, G. Enhancement of Circular Dichroism of a Chiral Material by Dielectric Nanospheres. J. Phys. Chem. C 2019, 123, 5017–5022.
- (24) Maoz, B. M.; Chaikin, Y.; Tesler, A. B.; Elli, O. B.; Fan, Z.; Govorov, A. O.; Markovich, G. Amplification of chiroptical activity of chiral biomolecules by surface plasmons. Nano Lett. 2013, 13, 1203–1209.
- (25) Lemesle-Lamache, V.; Wouessidjewe, D.; Chéron, M.; Duchêne, D. Study of β -cyclodextrin and ethylated β -cyclodextrin salbutamol complexes, in vitro evaluation of sustained-release behaviour of salbutamol. Int. J. Pharm. 1996, 141, 117–124.
- (26) Mitscher, L. A.; Kautz, F.; LaPidus, J. Optical rotatory dispersion and circular dichroism of diastereoisomers. I. The ephedrines and chloramphenicols. Can. J. Chem. 1969, 47, 1957–1963.
- (27) Kirkpatrick, D.; Fain, M.; Yang, J.; Trehy, M. Enantiomeric impurity analysis using circular dichroism spectroscopy with United States Pharmacopeia liquid chromatographic methods. J. Pharm. Biomed. Anal. 2018, 156, 366–371.
- (28) Okuom, M. O.; Burks, R.; Naylor, C.; Holmes, A. E. Applied Circular Dichroism: A Facile Spectroscopic Tool for Configurational Assignment and Determination of Enantiopurity. J. Anal. Methods Chem. 2015, 2015, 1–6.
- (29) Wenzel, S.; Buss, V. Circular dichroism and electronic structure calculations on naproxen. J. Phys. Org. Chem. 1992, 5, 748–754.
- (30) Puri, M.; Ferry, V. E. Circular Dichroism of CdSe Nanocrystals Bound by Chiral Carboxylic Acids. ACS Nano 2017, 11, 12240–12246.
- (31) García-Guirado, J.; Svedendahl, M.; Puigdollers, J.; Quidant, R. Enantiomer-Selective Molecular Sensing Using Racemic Nanoplasmonic Arrays. Nano Lett. 2018, 18, 6279–6285.
- (32) Lee, S.; Yoo, S.; Park, Q.-H. Microscopic Origin of Surface-Enhanced Circular Dichroism. ACS Photonics 2017, 4, 2047–2052.

(33) Mohammadi, E.; Tavakoli, A.; Dehkhoda, P.; Jahani, Y.; Tsakmakidis, K. L.; Tittl, A.; Altug, H. Accessible Superchiral Near-Fields Driven by Tailored Electric and Magnetic Resonances in All-Dielectric Nanostructures. ACS Photonics 2019, 6, 1939–1946.

- (34) Huang, T.-Y.; Grote, R. R.; Mann, S. A.; Hopper, D. A.; Exarhos, A. L.; Lopez, G. G.; Kaighn, G. R.; Garnett, E. C.; Bassett, L. C. A monolithic immersion metalens for imaging solid-state quantum emitters. Nat. Commun. 2019, 10, 2392.
- (35) Zhang, J. L.; Lagoudakis, K. G.; Tzeng, Y.-K.; Dory, C.; Radulaski, M.; Kelaita, Y.; Fischer, K. A.; Sun, S.; Shen, Z.-X.; Melosh, N. A.; Chu, S.; Vučković, J. Complete coherent control of silicon vacancies in diamond nanopillars containing single defect centers. Optica 2017, 4, 1317.
- (36) Evlyukhin, A. B.; Reinhardt, C.; Chichkov, B. N. Multipole light scattering by nonspherical nanoparticles in the discrete dipole approximation. Phys. Rev. B: Condens. Matter Mater. Phys. 2011, 84, 235429.
- (37) Staude, I.; Miroshnichenko, A. E.; Decker, M.; Fofang, N. T.; Liu, S.; Gonzales, E.; Dominguez, J.; Luk, T. S.; Neshev, D. N.; Brener, I.; Kivshar, Y. Tailoring Directional Scattering through Magnetic and Electric Resonances in Subwavelength Silicon Nanodisks. ACS Nano 2013, 7, 7824–7832.
- (38) Phillip, H.; Taft, E. Kramers-Kronig Analysis of Reflectance Data for Diamond. Phys. Rev. 1964, 136, A1445.
- (39) Kerker, M.; Wang, D.; Giles, C. Electromagnetic scattering by magnetic spheres. J. Opt. Soc. Am. 1983, 73, 765–767.
- (40) Zambrana-Puyalto, X.; Fernandez-Corbaton, I.; Juan, M.; Vidal, X.; Molina-Terriza, G. Duality symmetry and Kerker conditions. Opt. Lett. 2013, 38, 1857–1859.
- (41) Lawrence, M.; Dionne, J. A. Nanoscale nonreciprocity via photon-spin-polarized stimulated Raman scattering. Nat. Commun. 2019, 10, 3297.
- (42) Wan, N. H.; Mouradian, S.; Englund, D. Two-dimensional photonic crystal slab nanocavities on bulk single-crystal diamond. Appl. Phys. Lett. 2018, 112, 141102.
- (43) Kuhn, W.; Knopf, E. Z. Phys. Chem., Abt. B 1930, 7, 292.
- (44) Kuhn, W.; Lehmann, H. L. Z. Elektrochem 1939, 37, 549.
- (45) Fan, S.; Suh, W.; Joannopoulos, J. Temporal coupled-mode theory for the Fano resonance in optical resonators. J. Opt. Soc. Am. A 2003, 20, 569–572.
- (46) Overvig, A. C.; Shrestha, S.; Yu, N. Dimereized high contrast gratings. Nanophotonics 2018, 7, 1157–1168.
- (47) Koshelev, K.; Lepeshov, S.; Liu, M.; Bogdanov, A.; Kivshar, Y. Asymmetric Metasurfaces with High-Q Resonances Governed by Bound States in the Continuum. Phys. Rev. Lett. 2018, 121, 193903.
- (48) Strauf, S.; Rakher, M.; Carmeli, I.; Hennessy, K.; Meier, C.; Badolato, A.; DeDood, M.; Petroff, P.; Hu, E.; Gwinn, E.; Bouwmeester, D. Frequency control of photonic crystal membrane resonators by monolayer deposition. Appl. Phys. Lett. 2006, 88, 043116.
- (49) Ruf, T.; Cardona, M.; Pickles, C.; Sussmann, R. Temperature dependence of the refractive index of diamond up to 925 K. Phys. Rev. B: Condens. Matter Mater. Phys. 2000, 62, 16578–16581.
- (50) Tittl, A.; Leitis, A.; Liu, M.; Yesilkoy, F.; Choi, D.-Y.; Neshev, D. N.; Kivshar, Y. S.; Altug, H. Imaging-based molecular barcoding with pixelated dielectric metasurfaces. Science 2018, 360, 1105–1109.